



UNIVERSITY OF LEEDS

This is a repository copy of *Lithological Controls on Soil Aggregates and Minerals Regulate Microbial Carbon Use Efficiency and Necromass Stability*.

White Rose Research Online URL for this paper:

<https://eprints.whiterose.ac.uk/221815/>

Version: Accepted Version

Article:

Hu, P., Zhang, W., Nottingham, A.T. orcid.org/0000-0001-9421-8972 et al. (9 more authors) (2024) *Lithological Controls on Soil Aggregates and Minerals Regulate Microbial Carbon Use Efficiency and Necromass Stability*. *Environmental Science and Technology*, 58 (48). pp. 21186-21199. ISSN 0013-936X

<https://doi.org/10.1021/acs.est.4c07264>

This is an author produced version of an article published in *Environmental Science & Technology (ES&T)*, made available under the terms of the Creative Commons Attribution License (CC-BY), which permits unrestricted use, distribution and reproduction in any medium, provided the original work is properly cited.

Reuse

This article is distributed under the terms of the Creative Commons Attribution (CC BY) licence. This licence allows you to distribute, remix, tweak, and build upon the work, even commercially, as long as you credit the authors for the original work. More information and the full terms of the licence here:

<https://creativecommons.org/licenses/>

Takedown

If you consider content in White Rose Research Online to be in breach of UK law, please notify us by emailing eprints@whiterose.ac.uk including the URL of the record and the reason for the withdrawal request.



eprints@whiterose.ac.uk
<https://eprints.whiterose.ac.uk/>

Lithological controls on soil aggregates and minerals regulate microbial carbon use efficiency and necromass stability

Peilei Hu^{1,2,3}, Wei Zhang^{1,2,3*}, Andrew T. Nottingham^{4,5}, Dan Xiao^{1,2}, Yakov Kuzyakov^{6,7,8}, Lin Xu^{1,2,9}, Hongsong Chen^{1,2}, Jun Xiao^{1,2,3}, Pengpeng Duan^{1,2}, Tiangang Tang^{1,2}, Jie Zhao^{1,2,3}, Kelin Wang^{1,2*}

¹ Key Laboratory of Agro-Ecological Processes in Subtropical Region, Institute of Subtropical Agriculture, Chinese Academy of Sciences, Changsha 410125, China

² Huanjiang Agriculture Ecosystem Observation and Research Station of Guangxi, Guangxi Key Laboratory of Karst Ecological Processes and Services, Huanjiang Observation and Research Station for Karst Ecosystems, Chinese Academy of Sciences, Huanjiang 547100, China

³ Guangxi Industrial Technology Research Institute for Karst Rocky Desertification Control, Nanning 530000, China

⁴ School of Geography, University of Leeds, Leeds LS2 9JT, UK

⁵ Smithsonian Tropical Research Institute, Panama City 0843-03092, Republic of Panama

⁶ Department of Soil Science of Temperate Ecosystems, Department of Agricultural Soil Science, University of Goettingen, Göttingen 37077, Germany

⁷ Peoples Friendship University of Russia (RUDN University), Moscow 117198, Russia

⁸ Institute of Environmental Sciences, Kazan Federal University, Kazan 420049,

Russia

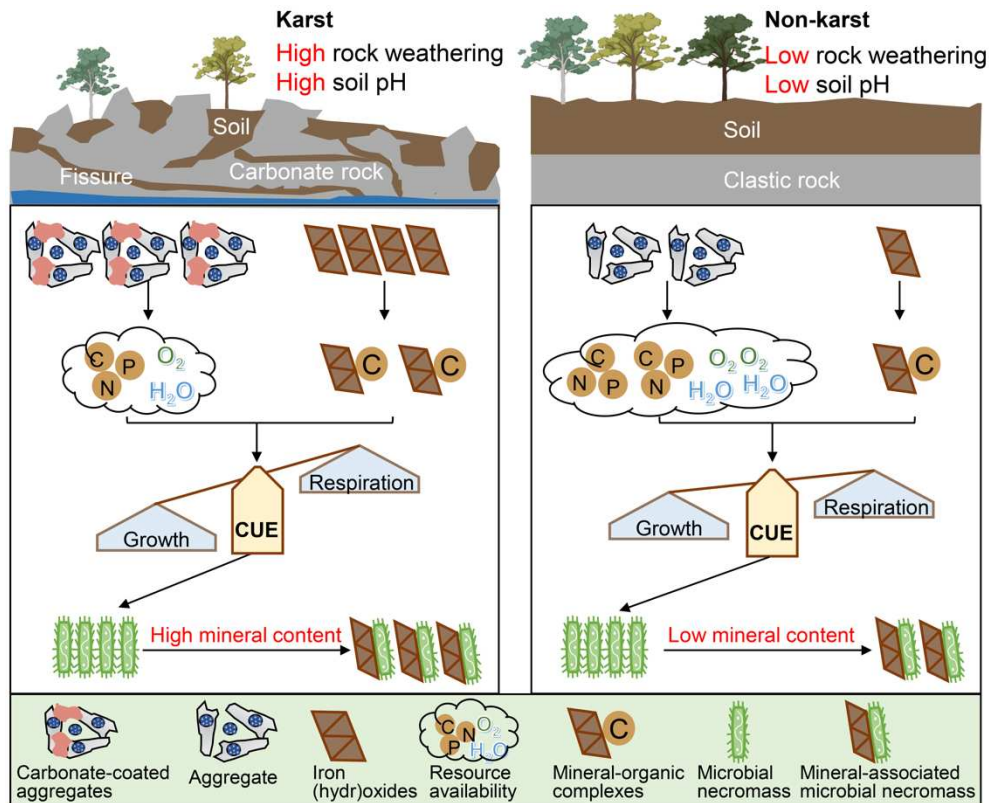
⁹ University of Chinese Academy of Sciences, Beijing 100049, China

* Email: zhangw@isa.ac.cn (Wei Zhang); Phone: 86-0731-84619720

* Email: kelin@isa.ac.cn (Kelin Wang); Phone: 86-0731-84615201

KEYWORDS

aggregates, iron (hydr)oxides, lithology, microbial life strategies, microbial
necromass, mineral protection



Graphic Abstract

ABSTRACT

Microbial carbon (C) use efficiency (CUE) drives soil C formation, while physical-chemical protection stabilizes subsequent microbial necromass, both shaped by soil aggregates and minerals. Soils inherit many properties from the parent material, yet the influence of lithology and associated soil geochemistry on microbial CUE and necromass stabilization remains unknown. Here, we quantified microbial CUE in well-aggregated bulk soils and crushed aggregates, as well as microbial necromass in bulk soils and the mineral-associated organic matter fraction, originating from carbonate-containing (karst) and carbonate-free (clastic rock, non-karst) parent materials along a broad climatic gradient. We found that aggregate crushing significantly increased microbial CUE in both karst and non-karst soils. Additionally, compared to non-karst

soils, calcium-rich karst soils increased macroaggregate stability and decreased the ratio of oligotrophic to copiotrophic microbial taxa, leading to a reduction in microbial CUE. Moreover, microbial CUE was negatively associated with iron (hydr)oxides in karst soils, attributed to the greater abundance of iron (hydr)oxides and higher soil pH. Despite the negative effects of soil aggregation and minerals on microbial CUE, particularly in karst soils, these soils concurrently showed greater microbial necromass stability through organo-mineral associations compared to non-karst soils. Consequently, i) bedrock lithology mediates the effects of aggregates and minerals on microbial CUE and necromass stability; and ii) balancing minerals' dual roles in diminishing microbial CUE and enhancing microbial necromass stability is vital for optimizing soil C preservation.

Synopsis

This study reveals that soil aggregation and minerals decrease microbial CUE and necromass production while increasing necromass stability, highlighting the need to balance these factors for effective carbon sequestration.

1 INTRODUCTION

Soil organic carbon (SOC) forms the largest carbon (C) pool in terrestrial ecosystems, profoundly influencing the climate¹ and ecosystem functioning.^{2,3} Microbial C use efficiency (CUE), defined as the proportion of assimilated C that remains retained in the microbial biomass, provides an integrative metric of microbial community metabolic regulation of organic C transformation in soils.⁴ A high CUE implies microbes allocate more C to biomass formation and resulting necromass production.⁵ While microbial CUE promotes SOC formation,⁴ the stabilization of subsequent microbial necromass regulates long-term soil C preservation.⁶ Therefore, microbially-mediated SOC storage relies on both the production and stabilization of microbial necromass. However, current research often isolates factors influencing either microbial CUE or necromass stability, neglecting their integration.

Soil aggregates have a large influence on microbial CUE, by shaping the physical structure of soil habitat and affecting resource availability and microbial community dynamics.⁷ For example, increased soil aggregation reduces nutrient availability, resulting in microbes allocating more energy for nutrient acquisition and losing more C in respiration.⁸ Additionally, aggregates and the associated pores create diverse microhabitats, influencing moisture as well as the quantity and quality of organic substrates.⁹ These aggregate-scale microhabitats shape soil microbial communities in terms of abundance, diversity, and life strategies (e.g. oligotrophic and copiotrophic strategists).¹⁰ The diverse energy maintenance requirements of microbial taxa result in differing CUE¹¹ and energy use efficiency.¹² Therefore, it is crucial to identify the effect

of aggregates on microbial CUE.

In parallel, soil minerals like iron (Fe) (hydr)oxides and calcium (Ca) not only shape soil structure¹³ but also determine microbial metabolic processes¹⁴ and can stabilize microbial necromass as mineral-associated organic matter (MAOM).¹⁵ However, the effect of minerals on microbial CUE and C storage is complex and dualistic. On one hand, high abundance of Fe (hydr)oxides and Ca can increase SOC accrual by stabilizing microbial products (i.e. necromass) in mineral–organic associations,^{16,17} contributing to the long-term persistence of SOC.¹⁸ On the other hand, these mineral–organic associations can also hinder SOC accrual, by decreasing substrate accessibility, increasing substrate limitation to microbes and thereby increasing microbial C allocation to extracellular enzyme synthesis for substrate acquisition, thereby reducing CUE.¹⁹ This reduction in CUE is considered to be negatively related to the SOC balance.⁴ The complex and dualistic influence of minerals on CUE and C accrual underscores the importance of studying these influences under different environmental conditions, especially under varying mineral preservation capacities.

Thus, we posit that variations in soil aggregates and minerals may have a major influence on microbial CUE and necromass stability,¹⁴ with differences in lithology of parent materials likely being a key source of this variation. The diversity of bedrock lithologies and rates of rock weathering affect biogeochemical cycles, by determining nutrient availability, mineral formation, organo-mineral associations, and aggregation.^{20,21} Theoretically, lithology influences microbial CUE and soil C storage

through a two-step process: i) regulating CUE by affecting the content and saturation status of soil minerals, as well as the structure and stability of soil aggregates; and ii) influencing microbial product stabilization through physical-chemical protection by aggregates and minerals. Nevertheless, the influence of lithology and associated soil geochemistry on microbial CUE and necromass stability remains unclear.

Here, we assessed how soil aggregates and minerals influence microbial CUE and necromass stability in strongly contrasting soils, derived from carbonate-containing (karst) and carbonate-free (clastic rock, non-karst) parent materials across different climates. Further, to test the influence of soil aggregation on CUE, we subjected these soils to two physical manipulations: well-aggregated bulk and crushed aggregate soils. We also explored whether there exist trade-offs between microbial- and mineral-driven C accumulation by examining the relationships between microbial CUE, necromass, and soil minerals across the two contrasting lithologies. We hypothesized that macroaggregates and minerals have a larger effect in reducing microbial CUE in karst soils compared to non-karst soils. This is attributed to the rapid kinetics associated with carbonate rocks, which leads to faster dissolution rates than those of clastic rocks.²² Consequently, this promotes the release of essential rock-derived nutrients such as Ca and Fe into the soil. These processes facilitate the accumulation of secondary Ca and Fe minerals, enhancing the stability of macroaggregates²³ and fostering the formation of organic-mineral associations.²⁴ We also hypothesized that despite reduced CUE resulting from aggregates and minerals in karst soils, the abundant Ca and Fe contents would promote stable necromass-mineral associations. Thus, we hypothesized that

there is a trade-off in the influence of aggregates and minerals on soil C balance, decreasing CUE and necromass production but increasing the stability of these necromass in soil.

2 MATERIALS AND METHODS

2.1 Site description and experimental design

The karst region in southwest China, spanning over 0.54 million km², represents one of the largest continuously exposed carbonate rock areas globally.²⁵ The karst ecosystems are predominantly composed of carbonate rocks such as limestone, dolomite, and their mixtures, which are much more soluble than most other bedrocks. This leads to the formation of thin and discontinuous soil horizons, cracks and holes in the rock, resulting in strong water limitation and low vegetation productivity.²⁶ In contrast, non-karst ecosystems in the region are primarily composed of clastic rocks, which are rich in silicon (Si) and contain very low in soluble components, making them highly resistant to weathering. Over the past half-century, the karst regions experienced strong environmental degradation due to population pressure and limited environmental carrying capacity.²⁵ However, with the implementation of ecological restoration projects, the region is now recognized as a "Greening Earth" hotspot and a major contributor to China's vegetation C sink.²⁷

The region has a subtropical monsoon climate, with a wide range in mean annual temperature (MAT) varying from 12 °C to 24 °C and mean annual precipitation (MAP) generally exceeding 1000 mm. This range of MAT and MAP is attributed to the region's

wide range in elevation (from <500 m to >3000 m above sea level) and latitude.²⁵ Given the gradient in both climate and geology (carbonate to clastic rocks), the karst region provides an ideal system to explore how geology determines microbial CUE and necromass stability.

The study was conducted along a north-to-south transect in Chongqing, Guizhou, and Guangxi provinces (21°84'–29°11' N, 106°93'–108°75' E) of southwest China. Six areas with distinct climatic gradients were selected along the transect. Sampling sites were established in secondary forests over carbonate rocks (karst) and clastic rocks (non-karst) in each area (Fig. 1). To ensure comparability among the sampling sites, the following criteria were implemented before establishing the sample plots. First, the bedrock type of the karst sites was confirmed to be carbonate rocks, while the non-karst sites was confirmed to be clastic rocks. This determination was made by initially referring to the lithological geological map to identify potential sample sites over carbonate and clastic rocks in each area. Subsequently, unweathered bedrock samples were collected from these sites to analyze their chemical properties and confirm the bedrock lithology (Fig. 1b). Second, the forests over both bedrock types had similar land-use history and stand age. All selected secondary forests were subject to extensive deforestation before the 1960s, after which they regenerated naturally and reached an estimated age of 60 ± 5 years at the time of sampling. The land-use history information for the selected forests was provided by the local forestry administration.

In each area, five large sampling plots (20 × 30 m) were established. The five sampling plots were generally located within a 1000 × 1000 m sampling square, with a

minimum distance of 20 m between them. In some cases, to meet bedrock and forest criteria, the distance between plots exceeded 1 kilometer. In total, 60 plots were established, comprising six areas, two bedrock types, and five replicates. The MAT of the sampling sites ranged from 11.4 °C to 21.7 °C, while the MAP ranged from 1165 mm to 1878 mm. Climate data were extracted from a high-resolution ($1/24^\circ$, ~ 4 km) global dataset of monthly climate provided by the TerraClimate database.²⁸ Detailed information on the sampling sites, including latitude, longitude, and dominant plant species can be found in Supplementary Table 1.

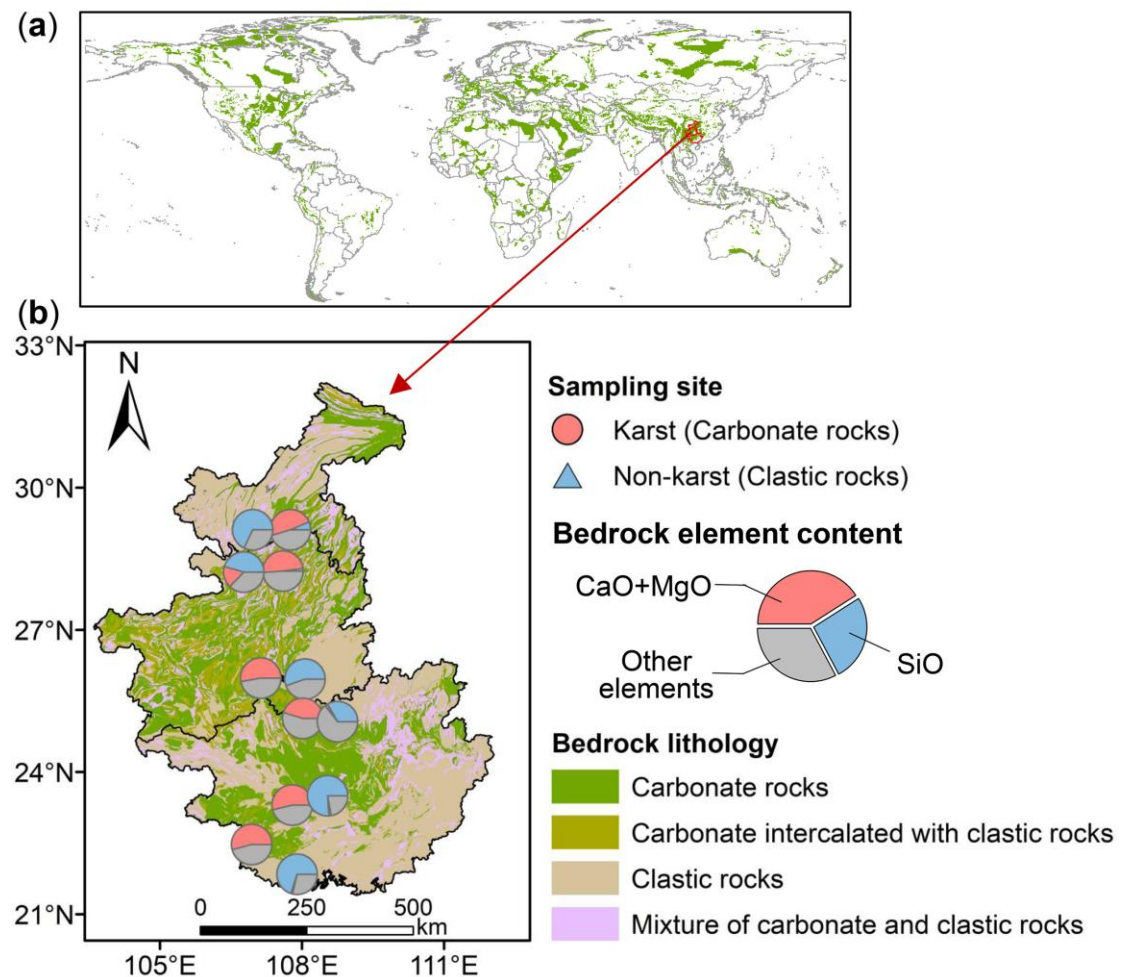


Fig. 1 Geographic overview of the sampling sites overlying carbonate rocks (karst) and clastic rocks (non-karst). **(a)** Spatial distribution of carbonate rocks globally and the study region; **(b)** bedrock

geochemical composition of the sampling sites. The colors within the pie charts in (b) represent the element contents of the bedrock.

2.2 Rock sampling and geochemical composition analysis

Within each plot, three to five minimally weathered rock samples were collected from intact bedrock outcrops and combined to represent the site's bedrock. In the laboratory, the outer weathered layer of each rock sample was removed using a lapidary slab saw. The unweathered rock samples were then subjected to a 24-hour cleaning process in 5% hydrogen peroxide to eliminate surface organic matter.²⁹ Afterward, the samples were heated to 105 °C to decompose any residual hydrogen peroxide. The cleaned rocks were subsequently crushed and ground to a particle size of 75 µm using a grinding machine. The elemental composition of the bedrock, including Si, Ca, and magnesium (Mg), was analyzed using an X-ray fluorescence spectrometer (Axios mAX, Malvern Panalytical B.V., Netherlands), with results expressed as the percentage content of SiO, CaO, and MgO, respectively.

2.3 Field sampling

In each plot, all individual woody plants with a diameter at breast height (DBH) \geq 1 cm (1.3 m above the forest floor) were identified, marked, and measured for DBH and tree height. Subsequently, 20 mineral soil cores (10 cm diameter, 0–10 cm depth) were collected from each plot using an S-shaped sampling method, following the removal of the organic layer. These soil cores were pooled to form composite samples.

Visible stones and roots were carefully removed. All soil samples were temporarily stored in iceboxes in the field and immediately transported to the laboratory.

In the laboratory, each soil sample was divided into three sub-samples using the quartering method. One part was stored at 4 °C for microbial C metabolism analyses, and another at –80 °C for microbial community structure analyses. All relevant measurements for the soil samples stored at both 4 °C and –80 °C were completed within two weeks. The remaining soil was naturally air-dried indoors at 25°C and then divided into three portions. One portion was used for soil aggregate fractionation, another for differentiating soil organic matter (SOM) into particulate organic matter (POM) and MAOM fractions, and the final portion for physicochemical property analyses.

2.4 Analysis of microbial C use efficiency

Microbial biomass C (MBC) and N (MBN) were determined using the chloroform fumigation-extraction method.³⁰ Then, to fully elucidate the effects of aggregates on CUE, both well-aggregated bulk soils and crushed aggregates were utilized to measure microbial CUE. The fresh soil, which passed through a 2 mm mesh sieve, was divided into two subsamples: one for well-aggregated soil and the other for crushed aggregates. For the crushed treatment, a ball mill (MM400; Retsch GmbH, Haan, Germany) was used to crush 10 g of soil per batch for 1 minute at a vibrational frequency of 250 min⁻¹, effectively breaking up the aggregates.³¹

Soil community-scale microbial CUE was determined using the substrate-

independent method based on the incorporation of $^{18}\text{O}\text{-H}_2\text{O}$ into microbial DNA.^{32,33} Briefly, both well-aggregated and crushed soils were preincubated in darkness at 25 °C for 7 days, maintaining soil moisture at 60% of their respective water holding capacity. Notably, the water holding capacity was measured separately for well-aggregated and crushed soils to ensure accurate comparisons. Subsequently, four replicates of each well-aggregated and crushed soils were prepared, with two tubes used for $^{18}\text{O}\text{-H}_2\text{O}$ labeling and the other two for unlabeled controls. For each replicate, 2 g of soil were placed into 2 mL centrifuge tubes. The tubes were then placed in 50 mL glass bottles, with four empty bottles serving as blanks. CO_2 -free air was then flushed into each bottle to ensure consistent initial gas conditions. The $^{18}\text{O}\text{-H}_2\text{O}$ (97 at% ^{18}O) was added to each of the two replicates, and the abundance was adjusted to 20 at% ^{18}O in the final soil water. The other two replicates received the same volume of unlabeled water to serve as natural abundance controls. After incubation at 25 °C for 24 hours, a 15 mL gas sample was collected from each bottle using a syringe, and the CO_2 concentration was determined using a gas chromatograph (GC-7890A; Agilent, Santa Clara, CA, USA). Microbial respiration rate (Respiration, $\mu\text{g C g}^{-1}\text{ soil h}^{-1}$) was calculated by determining the difference in headspace CO_2 concentration between the soil sample and blank (Equation 1).

$$\text{Respiration} = \frac{(C - C_0) * M * V * 273}{V_m * DW * 298 * t * 1000} \quad (1)$$

Where C and C_0 are the CO_2 concentrations (ppm) in the sample and blank, respectively; M is the molecular mass of the C (12 g mol^{-1}); V is the volume of the headspace in a bottle (mL); 273 is the absolute temperature (K) at standard atmospheric

pressure; V_m is the standard molar volume of ideal gas (L mol^{-1}); DW is the dry mass of soil (g); 298 is the incubation temperature (K); t is the incubation time (h); and 1000 is the unit conversion factor.

Microbial growth was calculated by tracking the incorporation of ^{18}O into microbial DNA through synthesis of new DNA. Total DNA was extracted from 0.5 g freeze-dried soil after incubation using the FastDNA Spin Kit (MP Biomedicals, Santa Ana, CA, USA) following the manufacturer's procedures. The quantity and quality of DNA were measured using a NanoDrop 2000 UV-VIS-spectrophotometer (Thermo Fisher Scientific, Wilmington, DE, USA). The remaining DNA extract was transferred into a silver cup and dried at 45 °C, after which the abundance of ^{18}O and the total O content were measured using a combined isotope ratio mass spectrometry and elemental analyzer equipment (IRMS/EA, Thermo Fisher, USA). During the 24-hour incubation, newly produced DNA ($\text{DNA}_{\text{produced}}$, μg) was quantified by the difference in ^{18}O abundance between the labelled and unlabeled samples (Equation 2)

$$\text{DNA}_{\text{produced}} = O_{\text{total}} * \frac{\text{at}\%_{\text{excess}}}{100} * \frac{100}{\text{at}\%_{\text{final}}} * \frac{100}{31.21} \quad (2)$$

where O_{total} is the total O content (μg) of the dried DNA extract; $\text{at}\%_{\text{excess}}$ is the difference between ^{18}O at% of the labelled and unlabeled sample; $\text{at}\%_{\text{final}}$ is the enrichment of ^{18}O at% of the final soil solution; and the constant 31.21 is the average proportional mass of O content in DNA ($\text{C}_{39}\text{H}_{44}\text{O}_{24}\text{N}_{15}\text{P}_4$).

The corresponding conversion factor (f_{DNA}) was calculated based on the ratio of MBC ($\mu\text{g g}^{-1}$ soil) to DNA content ($\mu\text{g g}^{-1}$ soil). Microbial growth rate (Growth, $\mu\text{g C g}^{-1}$ soil h^{-1}) was calculated based on the $\text{DNA}_{\text{produced}}$ and f_{DNA} (Equation 3).

$$Growth = \frac{f_{DNA} * DNA_{produced} * 1000}{DW * t * 1000} \quad (3)$$

Where DW is the dry mass of soil (g), and t is the incubation time (h).

Biomass-specific respiration ($Respiration_m$, mg C g⁻¹ MBC h⁻¹) and growth ($Growth_m$, mg C g⁻¹ MBC h⁻¹) were calculated based on microbial biomass (Equations 4 and 5).

$$Respiration_m = \frac{Respiration}{MBC} \quad (4)$$

$$Growth_m = \frac{Growth}{MBC} \quad (5)$$

Finally, microbial CUE was calculated based on growth and respiration (Equations 6).

$$CUE = \frac{Growth}{Growth + Respiration} \quad (6)$$

2.5 Analysis of microbial community structure

Soil microbial community structure, including bacterial and fungal abundance and community composition, was analyzed from fresh soil samples collected in the field and temporarily stored at -80°C. The DNA extraction method was consistent with that used for assessing microbial CUE. DNA quantity and quality were assessed with a NanoDrop 2000 UV-VIS spectrophotometer (Thermo Fisher Scientific, Wilmington, DE, USA). The abundance of bacterial 16S rRNA and fungal ITS genes was quantified using the 9600 Plus quantitative PCR system (Bioer Technology, Hangzhou, China). Primer pairs 341F (CCTAYGGGRBGCASCAG) and 806R (GGACTACHVGGGTWTCTAAT) were used for 16S rRNA gene amplification, while ITS1F (CTTGGTCATTTAGAGGAAGTAA) and ITS2R

(GCTGCGTTCTTCATCGATGC) were used for ITS gene amplification. The 20 μ L PCR reaction mixture contained 10 μ L of 2 \times ChamQ SYBR Color qPCR Master Mix, 0.4 μ L of each primer (5 μ M), 2 μ L of DNA template, and sterile ddH₂O. The PCR protocol was 5 min at 95 $^{\circ}$ C, followed by 40 cycles of 95 $^{\circ}$ C for 30 s, 56 $^{\circ}$ C for 30 s, and 72 $^{\circ}$ C for 40 s.

Bacterial and fungal community were determined by 16S and ITS gene amplicon sequencing, respectively. Amplification of the 16S rRNA gene sequences was achieved using the primer pair 338F (5'-ACTCCTACGGGAGGCAGCAG-3') and 806R (5'-GGACTACHVGGGTWTCTAAT-3'). For the ITS gene sequences, the primer pair ITS1F (5'-CTTGGTCATTTAGAGGAAGTAA-3') and ITS2R (5'-GCTGCGTTCTTCATCGATGC-3') were used. PCR mixtures contained dNTPs, FastPfu Buffer, primers, TaKaRa Taq DNA polymerase, BSA, template DNA, and sterile water. PCR was performed at 95 $^{\circ}$ C for 3 min, followed by 27 cycles for 16S rRNA and 35 cycles for ITS genes, each cycle consisting of 95 $^{\circ}$ C for 30 s, 55 $^{\circ}$ C for 30 s, and 72 $^{\circ}$ C for 45 s, ending with a final extension at 72 $^{\circ}$ C for 10 min. The products were sequenced using the Illumina MiSeq PE300 (Illumina, San Diego, CA, USA). The raw sequence data for 16S and ITS are openly accessible in the NCBI SRA under BioProject ID PRJNA1169648. The accession IDs for the data range from SAMN44080278 to SAMN44080401.

Sequencing data were analyzed using QIIME 2, with raw reads denoised via q2-dada2-plugin and unique sequences clustered into 97% identity OTUs using q2-vsearch. Taxonomic assignment for bacterial and fungal OTUs employed SILVA_v132³⁴ and

UNITE_v8.3³⁵ databases, respectively. Microbial α -diversity, quantified by the Shannon-Wiener index, was assessed using a rarefied ASV abundance table, with singletons and doubletons excluded to minimize sequencing noise. The calculation was conducted using the 'RAM' package in R (R Core Team, Vienna, Austria).

Classification of bacterial and fungal life strategies was based on phylum (or subphylum) level distinctions.^{36,37} For bacteria, phyla or subphylum such as Alphaproteobacteria, Deltaproteobacteria, Acidobacteria, Actinobacteria, Planctomycetes, and Chloroflexi were classified as likely oligotrophic phyla, whereas Gammaproteobacteria, Firmicutes, Gemmatimonadetes, and Bacteroidetes were classified as copiotrophic phyla.³⁸ For fungi, the phyla Basidiomycota and Ascomycota were classified as likely oligotrophic and copiotrophic phyla, respectively.³⁹ The ratio of oligotrophs to copiotrophs, calculated separately for bacteria and fungi, represents the quotient of the total relative abundance of oligotrophic phyla divided by the total relative abundance of copiotrophic phyla. We acknowledge the limitations of classifying microbial life strategies at the phylum (or subphylum) level, as diverse life strategies may coexist within specific phyla.^{38,40} However, given the current constraints in identification accuracy, we opted for phylum-level classifications, which can provide a broad approximation and generalization.⁴¹ We emphasize that these results should be interpreted with caution, and further research at finer taxonomic levels is essential to fully elucidate microbial life strategies.

2.6 Analysis of amino sugars

Microbial necromass C (MNC) content was quantified by analyzing amino sugars in both bulk soils and the MAOM fraction. We initially fractionated SOM into POM and MAOM forms.⁴² Briefly, we mixed 10 g of oven-dried soil with 50 mL of a solution containing 5 g L⁻¹ sodium hexametaphosphate and glass beads. The mixture was agitated on a reciprocating shaker for 18 hours to achieve comprehensive soil dispersion. After several rinses with distilled water, the fraction that passed through the 53- μ m mesh was collected as the MAOM fraction, while the materials retained on the mesh were identified as POM fraction. Subsequently, the POM and MAOM fractions underwent drying at 45°C until a constant weight was achieved.

Amino sugars were extracted using the following method.⁴³ Approximately 0.10 g of oven-dried soil (sample weight determined based on the corresponding total nitrogen [TN] content) underwent hydrolysis with 10 mL of 6 M HCl at 105 °C for 8 hours. An internal standard, myo-inositol, was added, and the solution underwent filtration and pH adjustment to 6.6–6.8 using KOH solution, followed by centrifugation for 10 min. The resulting supernatant was freeze-dried, and 5 mL of methanol was added to dissolve the residues. The solution was then dried using N₂ gas at 45 °C. Quantitative standard, N-methyl glucosamine, was added, and amino sugars were transformed into aldononitrile derivatives through heating in 0.3 mL of a derivatization reagent containing 32 mg mL⁻¹ of hydroxylamine hydrochloride and 40 mg mL⁻¹ of 4-(dimethylamino)-pyridine in a mixture of pyridine and methanol (4:1) at 75–80 °C for 35 min. Following cooling, the solution was reheated at 75–80 °C for 25 min for acetylation after the addition of 1 mL of acetic anhydride, followed by freeze-drying.

The removal of excessive derivatization reagents was done by extraction with 1 M HCl and deionized water. The dichloromethane phase containing amino sugar derivatives was then dried using N₂ gas at 45 °C. Prior to quantification, amino sugar derivatives were dissolved in 200 µL of ethyl acetate-hexane. Derivatives of amino sugars were analyzed using a gas chromatograph (GC-7890A; Agilent, Santa Clara, CA, USA) equipped with an HP-5 column and a flame ionization detector. Quantification employed internal standards to assess recovery efficiency during extraction procedures. We acknowledge that using myo-inositol recovery as a proxy for extraction efficiency has inherent limitations, as it may not fully capture the extraction efficiency of different amino sugars, particularly in soils with high pedogenic oxide content. Nevertheless, this approach remains the most widely accepted and utilized method for quantifying soil amino sugar content.

Amino sugars were quantified as glucosamine, galactosamine, and muramic acid. Muramic acid was used as a biomarker for bacterial necromass. Given that glucosamine is present in both fungal and bacterial cell walls, fungal-derived glucosamine was estimated based on the molar ratio of glucosamine to muramic acid of 2:1 in bacterial cells. Fungal and bacterial necromass C were calculated by multiplying the content of fungal-derived glucosamine by 9 and muramic acid by 45, respectively.⁴⁴ Total MNC was calculated as the sum of fungal and bacterial necromass C.

2.7 Soil aggregate separation

The soil aggregate size distribution was determined using wet sieving technique.³¹

Briefly, soil samples that were air-dried for a short period indoors (equivalent to 50 g dry weight) were submerged in deionized water for 5 min and then sieved successively over 250 μm and 53 μm sieves, with a shaking frequency of 30 times per minute for 30 minutes. The portion collected on the 250- μm sieve represented macroaggregates ($>250 \mu\text{m}$), while that collected on the 53- μm sieve represented microaggregates (53 to 250 μm). The remaining suspension ($<53 \mu\text{m}$) was considered silt + clay. Each fraction was then dried and weighted.

2.8 Soil physico-chemical properties

Soil exchangeable cations, such as Ca (Ca_{ex}) and Mg (Mg_{ex}), as well as calcium carbonate (CaCO_3) and Fe (hydr)oxides, were determined to represent soil minerals. Briefly, Ca_{ex} and Mg_{ex} were extracted using a 1 mol L^{-1} ammonium acetate.²⁴ Free Fe (hydr)oxides (Fe_d) represents pedogenic Fe and were extracted using the citrate-bicarbonate-dithionite (CBD) method.⁴⁵ Briefly, a solution of trisodium citrate and sodium bicarbonate was added to 0.50 g of soil and heated to 80 °C in a water bath. Sodium dithionite, the reducing agent, was then added, and the mixture was maintained at 80 °C for 15 minutes. After cooling, the solution was centrifuged, and the process was repeated multiple times to ensure complete extraction. The Fe content in the liquid extract was then measured. We chose the CBD method for two key reasons. First, preliminary experiments showed that in our study area, oxalate-extractable Fe accounted for a substantial proportion of Fe_d . Second, the high Ca content in karst soils means that CBD extraction not only captures oxalate-extractable Fe but also includes

Fe-OC-Ca complexes.⁴⁶ The contents of Ca_{ex} , Mg_{ex} , and Fe_d were determined using an inductively coupled plasma emission spectrometer (5110 ICP-OES; Agilent, Santa Clara, CA, USA).

Soil $CaCO_3$ content was determined by acid–base titration. In brief, after dissolving $CaCO_3$ with 0.5 mol L^{-1} HCl, the excess acid was titrated back with 0.2 mol L^{-1} NaOH to calculate the equivalent $CaCO_3$. Soil pH was determined using a pH electrode (FE20K, Mettler-Toledo, Switzerland) in a 1:2.5 soil-to-water suspension. SOC and TN in both bulk soils and the MAOM fraction were determined using an Elementar Vario MAX cube (Elementar, Hanau, Germany), with SOC being acidified using phosphoric acid prior to measurement.

2.9 Plant richness and biomass

Based on the vegetation survey data, plant α diversity, including richness and Shannon-Wiener diversity indices of tree species, was calculated using the “vegan” package in R. Aboveground biomass (AGB) was estimated using an allometric model with study site as dummy variable (Equation 7), which has been shown to be an effective approach for improving the accuracy of forest biomass estimations in subtropical China.⁴⁷ According to the 972 records of plot measured AGB in subtropical forest of China, a dummy variable allometric model was established,⁴⁷ and we used these parameters to calculate AGB (Equation 8).

$$AGB = \exp(a_0 + \sum a_i z_i + RSE^2 / 2) * (D^2 H)^b \quad (7)$$

$$AGB = \exp(-1.896 + 0.321 + 0.038) * (D^2 H)^{0.785} \quad (8)$$

where a_i is the site-specific parameter; z_i is the dummy variable (when $z_1 = 1$, the others = 0, when $z_2 = 1$, the others = 0, etc); RSE is the residual standard errors of the regressions; D is the diameter of the tree at breast height (cm); H is tree height (m); and a_0 and b are parameters.

2.10 Statistical analysis

We first assessed the normality and homogeneity of variance of the experimental data using the Shapiro-Wilk test and Levene's statistic, respectively, prior to conducting ANOVA. Natural log-transformation was applied where necessary to meet these criteria. The effects of lithology types (karst vs. non-karst) and aggregate structures (well-aggregated bulk soils vs. crushed aggregates), along with their interaction on microbial C metabolism (CUE, growth, and respiration), were investigated using two-way ANOVA (Table S2). We also explored the effect of lithology types on microbial C metabolism, plant properties (Shannon index and AGB), soil minerals (Ca_{ex} , Mg_{ex} , $CaCO_3$, and Fe_d), aggregates (macroaggregates and microaggregates), and microbial community structure (bacterial and fungal abundance, diversity, and life strategies) through independent samples t -tests. The effect of aggregate structures on microbial C metabolism was assessed via paired t -tests.

Ordinary least-squares regression was employed to assess the relationships of microbial CUE with climate (MAT and MAP), plant properties, soil minerals, and microbial community structure in karst and non-karst soils. Prior to conducting the regression analyses, we assessed the degree of autocorrelation between these variables

using Pearson's correlation coefficients (Fig. S1). Piecewise structural equation modelling (piecewiseSEM) was further utilized to dissect the direct and indirect relationships between CUE and the aforementioned variables. Based on prior knowledge, an initial hypothesized model was developed for evaluation (Fig. S2). Prior to inclusion in the SEM, variables within each group (e.g., climate, soil minerals, and microbial community structure) were amalgamated into "composite variable".⁴⁸ This analysis was performed using the "piecewiseSEM", "nlme", and "lme4" packages in R.

Lastly, we examined the relationship between microbial CUE and soil C storage, as well as the difference in soil C stability between karst and non-karst soils. Ordinary least-squares regression was used to explore the relationships between microbial CUE, SOC, MNC in bulk soils, and MNC in MAOM pool in karst and non-karst soils. Additionally, differences in soil C storage parameters (e.g., SOC, MNC, MAOM proportion, mineral-associated organic C, and mineral-associated MNC) between karst and non-karst soils were determined using independent samples *t*-tests.

3 RESULTS

3.1 Microbial C metabolism

In the well-aggregated bulk soils, MBC and microbial C metabolism parameters were similar between karst and non-karst soils (Fig. 2). However, aggregate crushing significantly affected all microbial C metabolism parameters (Table S2). In both soil types, microbial CUE, soil mass-based microbial growth and respiration, as well as biomass-specific growth and respiration, increased after crushing aggregates ($p < 0.01$,

Fig. 2b–f). Notably, the increase in microbial CUE and biomass-specific growth was greater in non-karst soils compared to karst soils ($p < 0.05$, Fig. 2b,d).

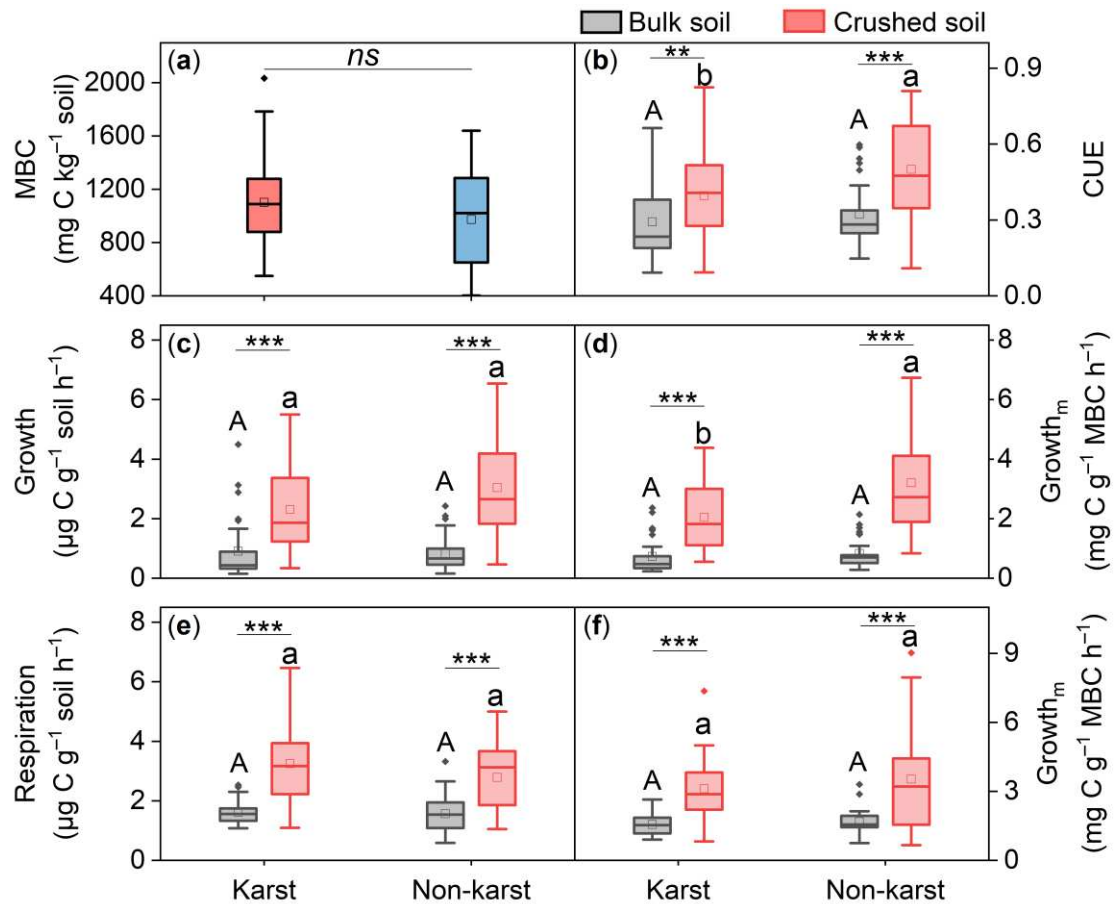


Fig. 2 Parameters of microbial C metabolism of well-aggregated bulk soils (Bulk soil) and crushed aggregates (Crushed soil) in karst and non-karst. (a) Microbial biomass C (MBC); (b) microbial C use efficiency (CUE); (c) soil mass-based microbial growth (Growth); (d) biomass-specific microbial growth (Growth_m); (e) soil mass-based microbial respiration (Respiration); and (f) biomass-specific microbial respiration (Respiration_m). The ends of the boxes represent the 25th and 75th percentiles, and the whiskers indicate 1.5 times the standard deviation. The central line and square represent the median and mean, respectively. Different capital letters and lowercase letters indicate significant differences ($p < 0.05$) between karst and non-karst for bulk soils and crushed soils, respectively, determined through independent samples *t*-tests. Asterisks indicate significant

differences between bulk soils and crushed soils within the same bedrock lithology from paired *t*-test. **, $p < 0.01$; ***, $p < 0.001$. *ns* indicates no significant difference ($p > 0.05$).

3.2 Associations of microbial CUE with abiotic and biotic factors

Microbial CUE was negatively associated with macroaggregate proportions in karst soils ($p < 0.001$) but increased with it in non-karst soils ($p < 0.05$, Fig. 3d). Mineralogy also influenced CUE, with a negative association between CUE and Fe_d in karst soils ($p < 0.001$), while no such relationship was observed in non-karst soils (Fig. 3e). Climatic factors consistently influence CUE across both soil types, with higher MAP and MAT associated with reduced CUE ($p < 0.05$; Fig. 3a–b).

In karst soils, both microbial diversity and life strategies were correlated with CUE. Bacteria diversity was positively correlated with CUE ($p < 0.05$, Fig. 3g), whereas fungal diversity was negatively correlated ($p < 0.01$, Fig. 3h). The ratio of oligotrophic to copiotrophic bacteria and fungi were positively associated with CUE ($p < 0.05$, Fig. 3k–l). In non-karst soils, only bacterial and fungal abundance were positively correlated with CUE ($p < 0.05$, Fig. 3i–j).

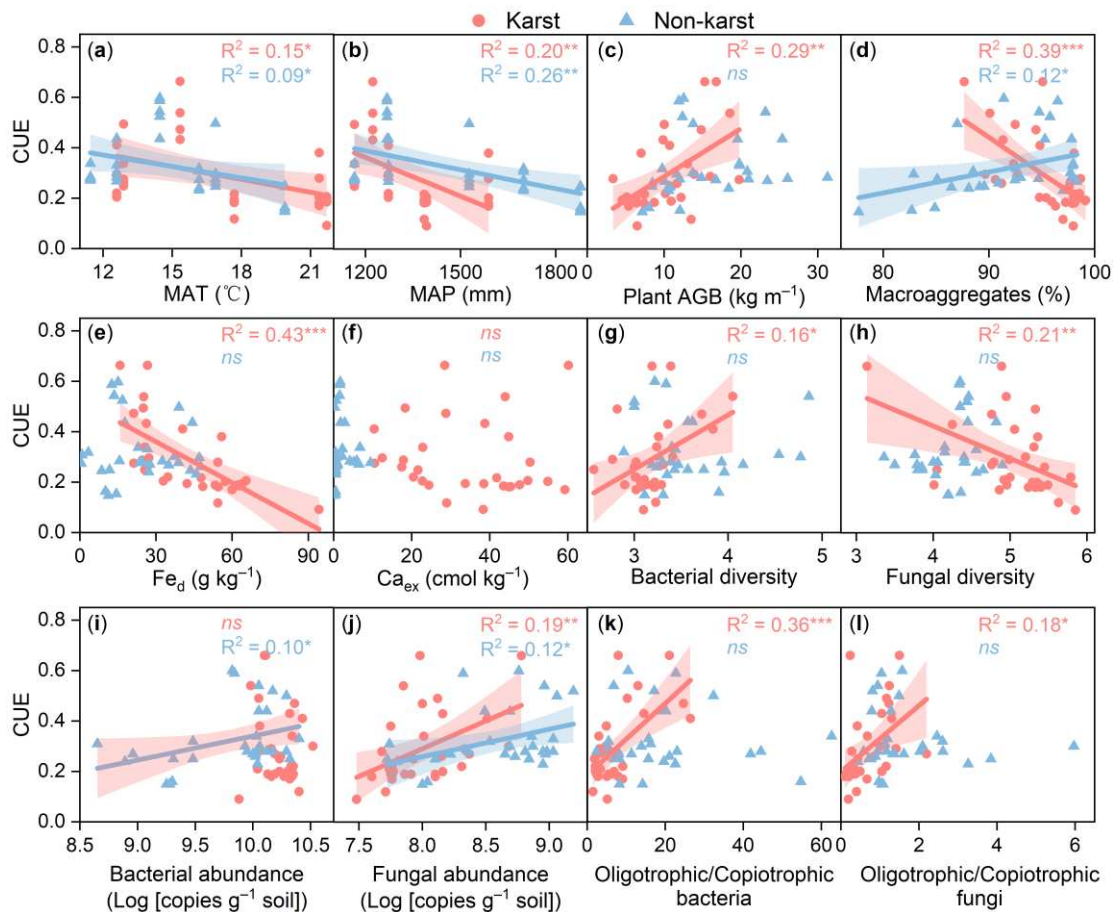


Fig. 3 Relationships of microbial C use efficiency (CUE) with climate, plant biomass, soil aggregates, minerals, and microbial community structure in karst and non-karst. Climate factors include (a) mean annual temperature (MAT) and (b) precipitation (MAP); plant biomass is represented by (c) aboveground biomass (AGB); soil aggregates are represented by (d) macroaggregate proportion; minerals include (e) dithionite-extractable Fe (hydr)oxides (Fe_d) and (f) exchangeable Ca (Ca_{ex}); and microbial community structure parameters include (g–h) bacterial and fungal diversity (Shannon-Wiener diversity index), (i–j) abundance (log₁₀-transformed), and (k–l) the ratio of oligotrophic to copiotrophic phyla. Solid lines represent regressions and shaded areas denote 95% confidence intervals. *, $p < 0.05$; **, $p < 0.01$; ***, $p < 0.001$. *ns* indicates no significant difference ($p > 0.05$).

PiecewiseSEM was used to assess the hypothesized direct and indirect relationships of microbial CUE with climate, plant biomass, soil minerals, macroaggregates, and microbial community structure. In karst soils, minerals and microbial community structure were directly associated with CUE, while macroaggregates were indirectly associated with CUE via microbial community structure (Fig. 4a). Climate and plant biomass indirectly influenced CUE by affecting minerals and macroaggregates (Fig. 4a). In non-karst soils, climate was identified as the sole factor directly and negatively associated with CUE (Fig. 4b).

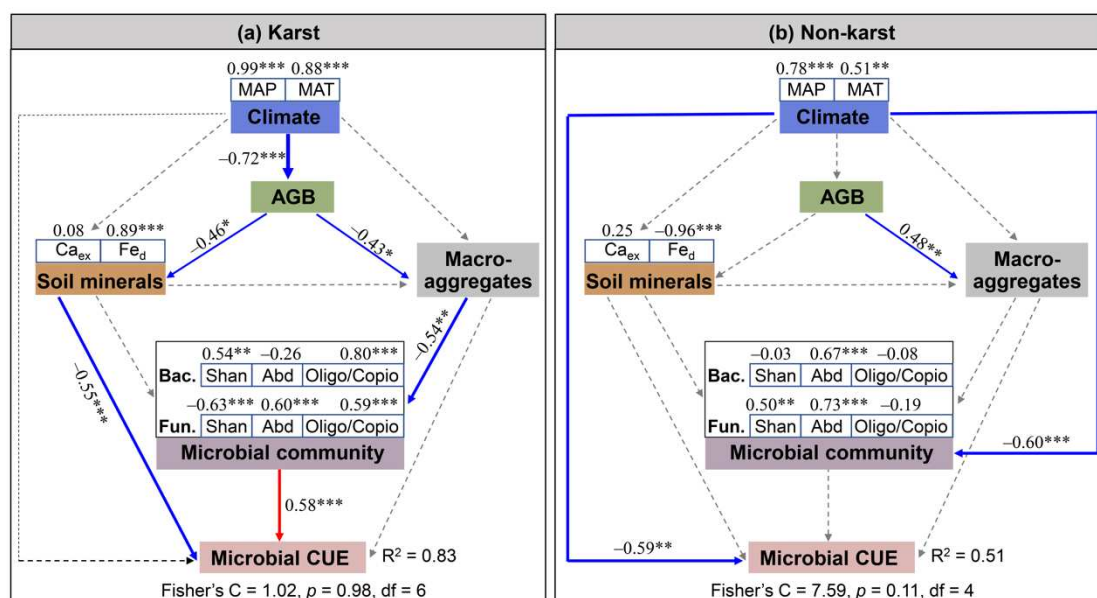


Fig. 4 Direct and indirect relationships between climate, plant biomass, soil minerals, macroaggregates, microbial community structure, and microbial C use efficiency (CUE) in (a) karst and (b) non-karst soils. The climate, soil minerals, and microbial community were divided into composite variable. Numbers adjacent to measured variables are their coefficients with the composite variable. Solid red and blue arrows represent positive and negative effects, respectively, while dashed arrows indicate non-significant paths ($p > 0.05$). Adjacent numbers represent standardized path coefficients, with arrow widths proportional to coefficient strengths. MAP, mean

annual precipitation; MAT, mean annual temperature; AGB, aboveground biomass; Ca_{ex} , exchangeable Ca; Fe_d , dithionite-extractable Fe; Shan, Shannon-Wiener diversity index; Abd, abundance; Oligo/Copio, the ratio of oligotrophic to copiotrophic phyla. *, $p < 0.05$; **, $p < 0.01$; ***, $p < 0.001$.

3.3 Microbial CUE, necromass production, and necromass stability

Soil mass-based microbial growth rate and CUE were positively correlated with the contents of SOC ($p < 0.05$) and MNC in the MAOM pool ($p < 0.01$) across both karst and non-karst soils (Fig. 5), indicating that both microbial growth and CUE contribute to necromass production in soils of different lithology. Despite similar SOC (Fig. S3a) and MNC contents (Fig. S4) between the two soil types, karst soils had a higher MAOM proportion ($p < 0.001$, Fig. 6a), as well as higher MAOC ($p < 0.001$, Fig. S3b) and mineral-associated MNC contents ($p < 0.001$, Fig. 6b). Additionally, mineral-associated MNC was positively correlated with Ca_{ex} in karst soils ($p < 0.05$, Fig. 6c) and with Fe_d in non-karst soils ($p < 0.05$, Fig. 6d). These results suggest that soil minerals enhance microbial necromass stability, particularly in karst soils rich in minerals.

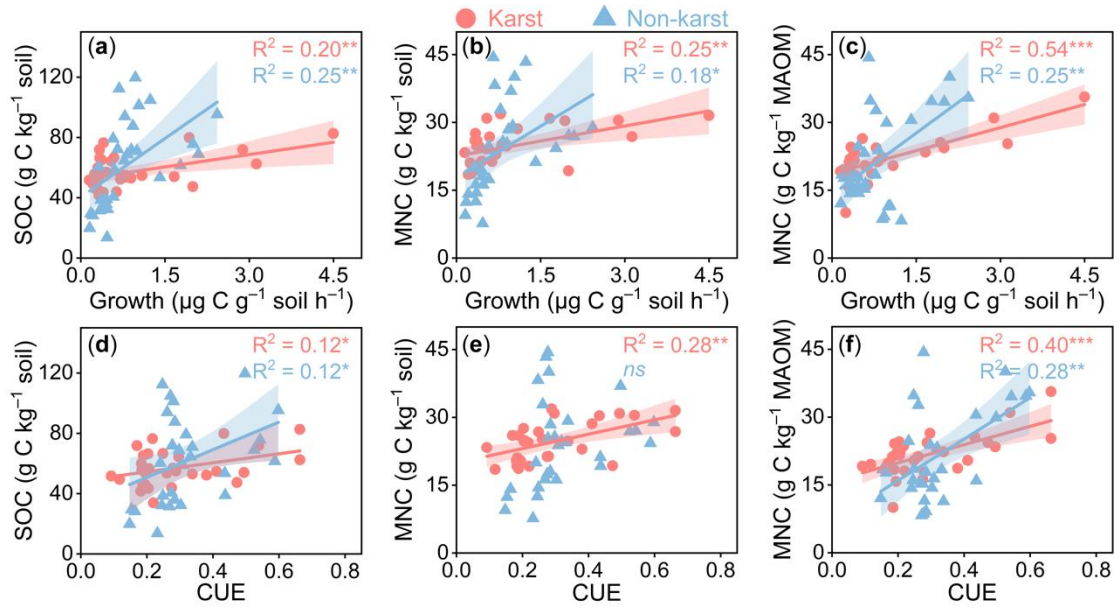


Fig. 5 Relationships of soil C accumulation with microbial growth rate and C use efficiency (CUE).

(a–c) Relationships of soil organic C (SOC), microbial necromass C (MNC) in bulk soils, and MNC in the mineral-associated organic matter (MAOM, <53 μm) pool with microbial growth rate. (d–f) Relationships of SOC, MNC in bulk soils, and MNC in the MAOM pool with microbial CUE. Solid lines represent regressions, and shaded areas denote 95% confidence intervals. *, $p < 0.05$; **, $p < 0.01$; and ***, $p < 0.001$. *ns* indicates no significant difference ($p > 0.05$).

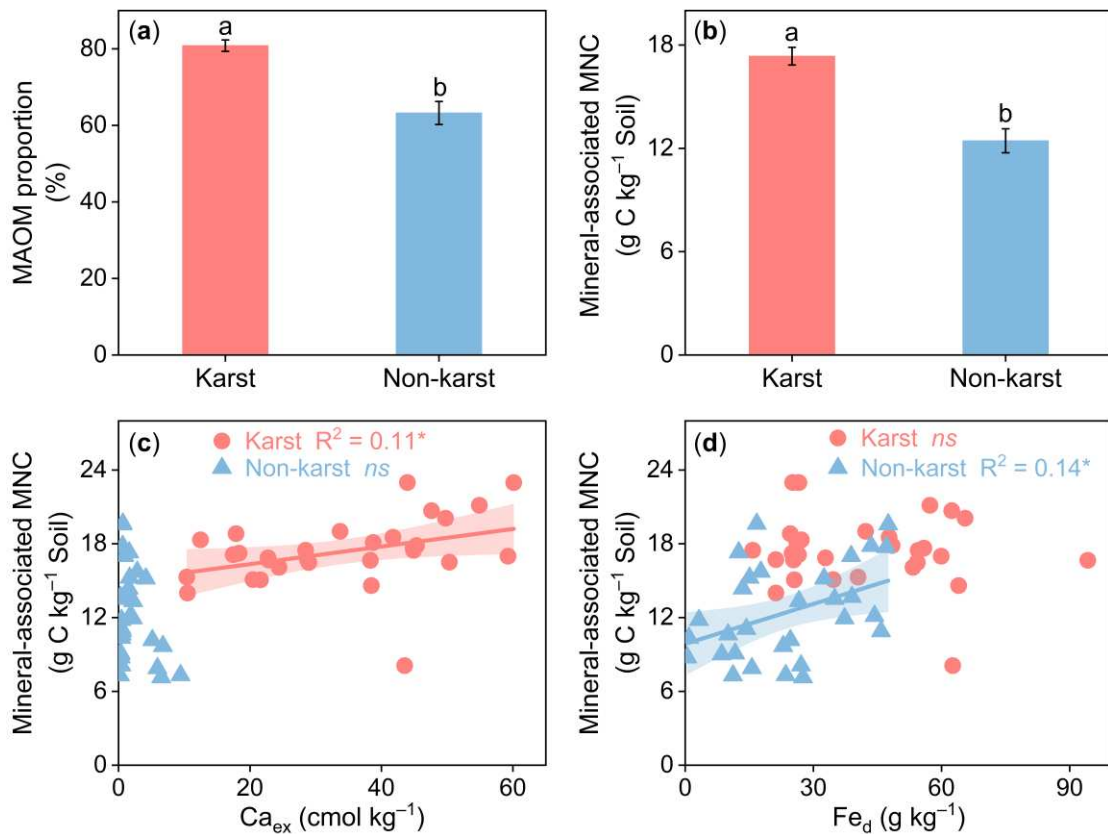


Fig. 6 Mineral-associated organic matter (MAOM) proportion and mineral-associated microbial necromass C (MNC) content, along with the relationship between mineral-associated MNC and soil minerals in karst and non-karst soils. In (a–b), the MAOM proportion and mineral-associated MNC content were compared between karst and non-karst soils from independent samples *t*-tests. The mineral-associated MNC content was calculated by multiplying the MNC content in the MAOM pool by the MAOM proportion. Lowercase letters indicate significant differences between karst and non-karst soils ($p < 0.001$). In (c–d), the relationships of mineral-associated MNC with soil exchangeable Ca (Ca_{ex}) and dithionite-extractable Fe (hydr)oxides (Fe_{d}) were assessed using regression analysis. Solid lines represent regressions, and shaded areas denote 95% confidence intervals. *, $p < 0.05$; and *ns* indicates no significant difference ($p > 0.05$).

4 DISCUSSION

We present compelling evidence supporting our hypothesis that soil aggregates and minerals exhibit a trade-off effect on soil C balance: they reduce microbial CUE while enhancing microbial necromass stability. Specifically, we found that decreased aggregation (by experimental crushing) strongly increased the CUE in both karst and non-karst soils (Fig. 2b). A negative correlation between microbial CUE and soil macroaggregate proportion was observed in karst soils (Fig. 3d). Additionally, a negative relationship between microbial CUE and Fe (hydr)oxides was found in karst soils (Fig. 3e, 4a), characterized by high Fe (hydr)oxides content (Table S3). Despite the negative effects of soil aggregation and minerals on microbial CUE, particularly in karst soils, these soils showed greater microbial necromass stability compared to non-karst soils. This was evidenced by the higher proportion of the MAOM fraction and increased mineral-associated MNC content (Fig. 6). Overall, our findings highlight the dual role of soil aggregates and minerals in shaping microbial CUE and necromass stability.

Aggregate crushing increased microbial CUE in both karst and non-karst soils (Fig. 2b), likely due to substrate release from organic matter and enhanced microbial activity.⁴⁹ A metabolic modeling study demonstrated that resource availability increases CUE, estimating a CUE of 0.3 ± 0.19 under resource-limiting conditions, which increased to 0.6 ± 0.17 in the absence of resource limitation.⁵⁰ Our experimental results align with these simulations, showing that crushing aggregates increased CUE from 0.29 to 0.40 in karst soils and from 0.32 to 0.50 in non-karst soils (Fig. 2b). An intriguing question arises as to why soil crushing had a greater effect on increasing CUE

in non-karst soils (56%) compared to karst soils (38%). This can be explained by the relative abundance of C in POM or MAOM of differing lithology. In the case of our experiment, the greater relative abundance of C in POM in non-karst soils resulted in a larger effect of aggregate disruption on increasing substrate availability and, in turn, CUE. Conversely, the greater relative abundance of C in MAOM in karst soils (Fig. S3b–c) maintain some degree of organic matter protection even after aggregate disruption. Thus, we posit that in soils with high MAOM abundance and low C accessibility, microbes allocate more C for extracellular enzyme synthesis, which constrains CUE and may explain low values of CUE reported in strongly weathered or tropical soils.^{4,51–53} Additionally, we posit that CUE in soils with greater relative abundance of C in MAOM is less affected by perturbation of soil aggregates.

The negative association between microbial CUE and higher macroaggregate proportion in karst soils could be attributed to the influence of soil Ca. In soils high in CaCO₃, such as karst soils, the continuous dissolution and local reprecipitation of CaCO₃ enhance the formation and stability of macroaggregates.⁵⁴ This occurs via the formation of secondary carbonate crystals, which can cement macroaggregates, increase the heterogeneity of matrix distribution, and decrease aggregate porosity.^{23,55} We observed that macroaggregate proportion in karst soils was positively correlated with Ca_{ex} and CaCO₃ (Fig. S5). Additionally, carbonate crystals were abundantly present on the surface of macroaggregates (Fig. S6). Consequently, high Ca content contributes to macroaggregate stability, causing microbes to invest more C in secreting extracellular enzymes, thereby reducing CUE. Furthermore, the continuous dissolution

and reprecipitation of CaCO_3 within macroaggregates create dynamic microsites, fostering environments favorable to copiotrophic microorganisms, which rapidly exploit short-lived resources and adapt to environmental fluctuations.^{41,56} Consistent with the viewpoint, we found that karst soils had higher abundances of bacterial and fungal copiotrophic phyla and lower ratios of oligotrophs to copiotrophs compared to non-karst soils (Fig. S7). Additionally, in karst soils, lower ratios of oligotrophs to copiotrophs were correlated with higher macroaggregate proportion (Fig. S8). Copiotrophic phyla, characterized by faster catabolic processes due to higher energy demand,⁵⁷ exhibit lower CUE compared to oligotrophic microorganisms.³⁸ Similarly, our results indicate that a reduction in the ratio of oligotrophs to copiotrophs correlated with lower microbial CUE (Fig. 3k–l; Fig. 4a). These findings suggest potential interactions among Ca, aggregation, and microbial community structure in decreasing microbial CUE.

Slightly different from our expectations, we found that microbial CUE was negatively correlated with Fe (hydr)oxides content only in karst soils, while no such correlation was observed in non-karst soils (Fig. 3e). This difference is likely due to the significantly higher Fe (hydr)oxides content in karst soils compared to non-karst soils (Table S3). The rapid weathering of carbonate rocks accelerates the accumulation of secondary minerals,²² including Ca and Fe (hydr)oxides, in these soils.²⁰ The abundant Ca and Fe minerals in karst soils enhance SOC protection, thereby limiting C availability for microbes.⁶ As a result, microbes allocate more C to synthesizing extracellular enzymes for C acquisition, rather than incorporating it into biomass, which

leads to lower CUE.¹⁹ Additionally, Fe minerals may hinder microbial colonization in karst soils. The surface charge of Fe (hydr)oxides, influenced by soil pH, affects microbial-mineral interactions.⁵⁸ With the pH of karst soils (6.6 ± 0.1) approaching ferrihydrite's zero charge point ($\text{pH} \geq 7$),⁵⁹ Fe (hydr)oxides likely carry neutral or negative charges, discouraging microbial colonization due to charge incompatibilities. Consequently, the association of SOC with Fe minerals and the surface characteristics of Fe (hydr)oxides in karst soils together contribute to the observed negative relationship between microbial CUE and Fe (hydr)oxides.

Besides the direct influence of soil aggregates and minerals, the role of climate in mediating microbial CUE should not be neglected. Our findings reveal a negative correlation between CUE and both MAT and MAP in karst and non-karst soils (Fig. 3a–b). In karst soils, higher temperatures and precipitation reduced CUE by lowering forest biomass, which in turn constrained the formation of soil macroaggregates and mineral accumulation (Fig. 4a). This can be attributed to a notable temperature differential ($\Delta\text{temperature} > 10\text{ }^\circ\text{C}$) in our study region, which amplifies evapotranspiration and exacerbates water stress.⁶⁰ These effects are particularly pronounced in karst landscapes, where extensive subterranean drainage networks amplify water loss,²⁶ leading to a decline in forest biomass. Reduced biomass diminishes the dissolution of Ca and Fe from bedrock and primary minerals, as well as macroaggregate formation, likely due to decreased root exudation.⁶¹ In contrast, in non-karst soils, higher temperatures and precipitation reduced microbial abundance and CUE (Fig. 4b), likely due to decreased soil nutrient availability.⁵³ Warmer temperatures and greater rainfall typically accelerate

organic matter decomposition and nutrient leaching, resulting in lower nutrient availability.⁶² Supporting this speculation, we observed negative correlations between soil nutrient availability and both temperature and precipitation (Fig. S9). Overall, these findings underscore the unneglectable role of climate in shaping microbial CUE.

As hypothesized, the higher mineral content in karst soils contributes to a higher content of mineral-associated microbial necromass C compared to non-karst soils (Fig. 6 a–b). Additionally, the positive correlation between mineral-associated microbial necromass C and minerals in both soil types (Fig. 6c–d) further supports the role of minerals in enhancing microbial necromass stability. Mineral protection contributes to soil C preservation primarily by restricting substrate availability and inhibiting microbial activity. Organic-mineral complexes are generally too large for microbial ingestion.¹⁸ Additionally, soil extracellular enzymes involved in SOM degradation have a strong affinity for mineral surfaces, and their activity diminishes after adsorption.⁶³ Despite microbial necromass production was positively correlated with microbial growth rate and CUE (Fig. 5), without mineral protection, necromass—comprising simple, nutrient-rich compounds—undergoes rapid microbial decomposition.⁶⁴ Unprotected microbial necromass can decompose 1000 times faster than the mineral-associated pool,⁶⁵ emphasizing the crucial role of necromass stabilization in SOC persistence.⁶⁶ Microbial turnover represents the initial stage of SOC accumulation, while microbial necromass stability reflects the subsequent stage. Together, these processes enhance soil C sequestration. Consequently, the dual role of minerals in influencing microbial CUE and necromass stability underscores the importance of

integrating the "microbial C pump" and "mineral C pump" concepts,^{15,18} given their synergies and trade-offs.

Our study establishes a framework for understanding the synergies and trade-offs between microbial- and mineral-driven C storage, but it has some limitations that warrant further investigation. First, while our study sites in southwest China capture a broad gradient in climate and geology,²⁵ expanding the research to other regions with diverse environmental conditions and bedrock distributions would enhance the generalizability of our findings. Second, although community-level analyses provide valuable insights into shifts in microbial structure and function, future studies should include keystone microbial taxa, microbial interactions, and functional genes to achieve a more comprehensive understanding of microbial-mediated soil C dynamics.¹⁴ Third, while our study identifies the roles of soil minerals in influencing microbial CUE and necromass stability, it is crucial to recognize the complexity and interconnectedness of these processes. A more robust approach would involve integrating field observations with laboratory simulations across varied environmental conditions.⁶⁷

Environmental Implications. Our results clearly demonstrate a trade-off in how soil aggregation and minerals affect SOC balance: while they decrease microbial growth rate, CUE, and necromass production, they simultaneously enhance the stability of microbial necromass. This trade-off is intensified by high mineral preservation capacity. Our findings suggest that relying solely on microbial processes underlying CUE to predict SOC feedbacks to climate change and to enhance SOC sequestration may be misleading. For example, a biogeochemical equilibrium model indicated that

microbial CUE in global farmland was higher than in forest soils.⁶⁸ This does not necessarily imply that farmland soils exhibit higher microbial C sequestration potential, as stabilization likely plays a more crucial role than production (CUE) in SOC accumulation.⁶⁶ Our findings also suggest that the underlying bedrock types and their associated weathering processes mediate the trade-offs between microbial necromass production and stabilization. Enhanced rock weathering, achieved by applying powdered silicate or carbonate rocks to the soil surface, accelerate natural weathering process. This strategy is recognized as effective for atmospheric CO₂ removal⁶⁹ and promoting SOC accumulation by releasing short-range-order minerals that enhance soil C stabilization.⁷⁰ However, increased mineral content also reduces microbial CUE, leading to more C being respired as CO₂. Therefore, practices involving enhanced rock weathering must consider both the mineralogy of the added rock powder and its application rate. This balance is essential to promote microbial necromass stabilization without significantly diminishing microbial CUE, thereby maximizing C sequestration potential.

ASSOCIATED CONTENT

Supporting information

Table S1. Geographical information, climate, and dominant plant species at the sampling sites.

Table S2. Effects of lithology types, aggregate structure, and their interaction on microbial carbon metabolism based on two-way ANOVA test.

Table S3. Plant and soil properties in karst and non-karst forests.

Fig. S1 Correlation matrix of environmental variables used to explain microbial carbon use efficiency.

Fig. S2 A initial conceptual model designed to infer the hypothesized direct and indirect relationships between climate, plant aboveground biomass, soil minerals, macroaggregates, microbial community structure, and microbial carbon use efficiency.

Fig. S3 Soil organic carbon and mineral-associated organic carbon contents, along with the proportion of MAOC to SOC, between karst and non-karst soils.

Fig. S4 Comparison of microbial necromass carbon contents in bulk soil and mineral-associated organic matter pool between karst and non-karst soils.

Fig. S5 Relationship between macroaggregate proportion and calcium content in karst soils.

Fig. S6 The exemplary morphology of macroaggregates in karst soils and the corresponding elemental composition within the crystal.

Fig. S7 The relative abundances of oligotrophic and copiotrophic bacteria and fungi, along with the ratio of oligotrophs to copiotrophs, between karst and non-karst soils.

Fig. S8 Relationship between the ratio of oligotrophs to copiotrophs and macroaggregate proportions in karst and non-karst soils.

Fig. S9 Relationships between soil nutrients and climate variables in non-karst soils.

AUTHOR INFORMATION

Corresponding Author

Wei Zhang (E-mail: zhangw@isa.ac.cn; Phone: 86-0731-84619720; ORCID: 0000-0003-4718-6386) and

Kelin Wang (E-mail: kelin@isa.ac.cn; Phone: 86-0731-84615201; ORCID: 0000-0001-8218-5368)

Author Contributions

Peilei Hu: Conceptualization, Formal Analysis, Visualization, Writing – Original Draft Preparation; **Wei Zhang:** Conceptualization, Funding Acquisition, Writing – Review & Editing; **Andrew T. Nottingham:** Writing – Review & Editing; **Dan Xiao:** Investigation, Visualization; **Yakov Kuzyakov:** Writing – Review & Editing; **Lin Xu:** Investigation; **Hongsong Chen:** Investigation, Supervision; **Jun Xiao:** Investigation; **Pengpeng Duan:** Investigation; **Tiangang Tang:** Investigation; **Jie Zhao:** Investigation; **Kelin Wang:** Conceptualization, Funding Acquisition, Writing – Review & Editing.

Notes

The authors declare no competing financial interests.

Acknowledgements

We thank the Institutional Center for Shared Technologies and Facilities of Institute of Subtropical Agriculture, CAS, for supporting the analyses of soil physical and chemical properties. This study was supported by the National Key Research and Development Program of China [2022YFF1300705], the Joint Funds of the National Natural Science

Foundation of China [U20A2011; U23A20155], the Science and Technology Innovation Program of Hunan Province [2022RC1016], the National Natural Science Foundation of China [42377351; 42207065], the RUDN University Strategic Academic Leadership Program, and the Strategic Academic Leadership Program "Priority 2030" of the Kazan Federal University.

References

- (1) Bossio, D. A.; Cook-Patton, S. C.; Ellis, P. W.; Fargione, J.; Sanderman, J.; Smith, P.; Wood, S.; Zomer, R. J.; von Unger, M.; Emmer, I. M.; Griscom, B. W. The role of soil carbon in natural climate solutions. *Nature Sustainability* **2020**, *3* (5), 391–398.
- (2) Kopittke, P. M.; Berhe, A. A.; Carrillo, Y.; Cavagnaro, T. R.; Chen, D.; Chen, Q. L.; Román Dobarco, M.; Dijkstra, F. A.; Field, D. J.; Grundy, M. J.; He, J. Z.; Hoyle, F. C.; Kögel-Knabner, I.; Lam, S. K.; Marschner, P.; Martinez, C.; McBratney, A. B.; McDonald-Madden, E.; Menzies, N. W.; Mosley, L. M.; Mueller, C. W.; Murphy, D. V.; Nielsen, U. N.; O'Donnell, A. G.; Pendall, E.; Pett-Ridge, J.; Rumpel, C.; Young, I. M.; Minasny, B. Ensuring planetary survival: the centrality of organic carbon in balancing the multifunctional nature of soils. *Critical Reviews in Environmental Science and Technology* **2022**, *52* (23), 4308–4324.
- (3) Minasny, B.; McBratney, A. B.; Arrouays, D.; Chabbi, A.; Field, D. J.; Kopittke, P. M.; Morgan, C. L.; Padarian, J.; Rumpel, C. Soil carbon sequestration: much more than a climate solution. *Environmental Science & Technology* **2023**, *57* (48), 19094–19098.
- (4) Tao, F.; Huang, Y.; Hungate, B. A.; Manzoni, S.; Frey, S. D.; Schmidt, M. W. I.; Reichstein, M.; Carvalhais, N.; Ciais, P.; Jiang, L.; Lehmann, J.; Wang, Y.P.; Houlton, B. Z.; Ahrens, B.; Mishra, U.;

Hugelius, G.; Hocking, T. D.; Lu, X.; Shi, Z.; Viatkin, K.; Vargas, R.; Yigini, Y.; Omuto, C.; Malik, A. A.; Peralta, G.; Cuevas-Corona, R.; Di Paolo, L. E.; Luotto, I.; Liao, C.; Liang, Y.S.; Saynes, V. S.; Huang, X.; Luo, Y. Microbial carbon use efficiency promotes global soil carbon storage. *Nature* **2023**, *618*, 981–985.

(5) Wang, C.; Qu, L.; Yang, L.; Liu, D.; Morrissey, E.; Miao, R.; Liu, Z.; Wang, Q.; Fang, Y.; Bai, E. Large-scale importance of microbial carbon use efficiency and necromass to soil organic carbon. *Global Change Biol* **2021**, *27* (10), 2039–2048.

(6) Hemingway, J. D.; Rothman, D. H.; Grant, K. E.; Rosengard, S. Z.; Eglinton, T. I.; Derry, L. A.; Galy, V. V. Mineral protection regulates long-term global preservation of natural organic carbon. *Nature* **2019**, *570* (7760), 228–231.

(7) Kravchenko, A.; Guber, A.; Gunina, A.; Dippold, M.; Kuzyakov, Y. Pore-scale view of microbial turnover: Combining ¹⁴C imaging, μ CT and zymography after adding soluble carbon to soil pores of specific sizes. *Eur J Soil Sci* **2021**, *72* (2), 593–607.

(8) Zhang, Q.; Qin, W.; Feng, J.; Zhu, B. Responses of soil microbial carbon use efficiency to warming: Review and prospects. *Soil Ecology Letters* **2022**, *4* (4), 307–318.

(9) Yudina, A.; Kuzyakov, Y. Dual nature of soil structure: The unity of aggregates and pores. *Geoderma* **2023**, *434*, 116478.

(10) Wilpsheski, R. L.; Aufrecht, J. A.; Retterer, S. T.; Sullivan, M. B.; Graham, D. E.; Pierce, E. M.; Zablocki, O. D.; Palumbo, A. V.; Elias, D. A. Soil Aggregate Microbial Communities: Towards Understanding Microbiome Interactions at Biologically Relevant Scales. *Appl. Environ. Microbiol.* **2019**, *85* (14), e00324-00319.

(11) Gunina, A.; Kuzyakov, Y. From energy to (soil organic) matter. *Global Change Biol* **2022**, *28*

(7), 2169–2182.

(12) Wang, C.; Kuzyakov, Y. Energy use efficiency of soil microorganisms: Driven by carbon recycling and reduction. *Global Change Biol* **2023**, *29* (22), 6170–6187.

(13) Eusterhues, K.; Rumpel, C.; Kögel-Knabner, I. Organo-mineral associations in sandy acid forest soils: importance of specific surface area, iron oxides and micropores. *Eur J Soil Sci* **2005**, *56* (6), 753–763.

(14) Sokol, N. W.; Slessarev, E.; Marschmann, G. L.; Nicolas, A.; Blazewicz, S. J.; Brodie, E. L.; Firestone, M. K.; Foley, M. M.; Hestrin, R.; Hungate, B. A.; Koch, B. J.; Stone, B. W.; Sullivan, M. B.; Zablocki, O.; Trubl, G.; McFarlane, K.; Stuart, R.; Nuccio, E.; Weber, P.; Jiao, Y.; Zavarin, M.; Kimbrel, J.; Morrison, K.; Adhikari, D.; Bhattacharaya, A.; Nico, P.; Tang, J.; Didonato, N.; Paša-Tolić, L.; Greenlon, A.; Sieradzki, E. T.; Dijkstra, P.; Schwartz, E.; Sachdeva, R.; Banfield, J.; Pett-Ridge, J.; Consortium, L. S. M. Life and death in the soil microbiome: how ecological processes influence biogeochemistry. *Nature Reviews Microbiology* **2022**, *20*, 415–430.

(15) Liang, C.; Schimel, J. P.; Jastrow, J. D. The importance of anabolism in microbial control over soil carbon storage. *Nature Microbiology* **2017**, *2* (8), 1–6.

(16) Li, Q.; Song, Z.; Xia, S.; Kuzyakov, Y.; Yu, C.; Fang, Y.; Chen, J.; Wang, Y.; Shi, Y.; Luo, Y.; Li, Y.; Chen, J.; Wang, W.; Zhang, J.; Fu, X.; Vancov, T.; Van Zwieten, L.; Liu, C.Q.; Wang, H. Microbial Necromass, Lignin, and Glycoproteins for Determining and Optimizing Blue Carbon Formation. *Environmental Science & Technology* **2024**, *58* (1), 468–479.

(17) He, H.; Liu, J.; Shu, Z.; Chen, Y.; Pan, Z.; Peng, C.; Wang, X.; Zhou, F.; Zhou, M.; Du, Z.; Sun, K.; Xing, B.; Wang, Z. Microbially Driven Iron Cycling Facilitates Organic Carbon Accrual in Decadal Biochar-Amended Soil. *Environmental Science & Technology* **2024**, *58* (28), 12430–12440.

- (18) Xiao, K.Q.; Zhao, Y.; Liang, C.; Zhao, M.; Moore, O. W.; Otero-Fariña, A.; Zhu, Y.G.; Johnson, K.; Peacock, C. L. Introducing the soil mineral carbon pump. *Nature Reviews Earth & Environment* **2023**, *4* (3), 135–136; DOI 10.1038/s43017-023-00396-y.
- (19) Feng, X.; Qin, S.; Zhang, D.; Chen, P.; Hu, J.; Wang, G.; Liu, Y.; Wei, B.; Li, Q.; Yang, Y.; Chen, L. Nitrogen input enhances microbial carbon use efficiency by altering plant–microbe–mineral interactions. *Global Change Biol* **2022**, *28* (16), 4845–4860.
- (20) Fang, Q.; Lu, A.; Hong, H.; Kuzyakov, Y.; Algeo, T. J.; Zhao, L.; Olshansky, Y.; Moravec, B.; Barrientes, D. M.; Chorover, J. Mineral weathering is linked to microbial priming in the critical zone. *Nature Communications* **2023**, *14* (1), 345.
- (21) Munroe, J. S.; Farrugia, G.; Ryan, P. C. Parent material and chemical weathering in alpine soils on Mt. Mansfield, Vermont, USA. *Catena* **2007**, *70* (1), 39–48.
- (22) Liu, Z.; Dreybrodt, W.; Liu, H. Atmospheric CO₂ sink: Silicate weathering or carbonate weathering? *Applied Geochemistry* **2011**, *26*, S292–S294.
- (23) Rowley, M. C.; Grand, S.; Verrecchia, É. P. Calcium-mediated stabilisation of soil organic carbon. *Biogeochemistry* **2018**, *137* (1-2), 27–49.
- (24) Hu, P.; Zhang, W.; Chen, H.; Xu, L.; Xiao, J.; Luo, Y.; Wang, K. Lithologic control of microbial-derived carbon in forest soils. *Soil Biology and Biochemistry* **2022**, *167*, 108600.
- (25) Wang, K.; Zhang, C.; Chen, H.; Yue, Y.; Zhang, W.; Zhang, M.; Qi, X.; Fu, Z. Karst landscapes of China: patterns, ecosystem processes and services. *Landscape Ecol* **2019**, *34*, 2743–2763.
- (26) Jiang, Z.; Liu, H. Y.; Wang, H. Y.; Peng, J.; Meersmans, J.; Green, S. M.; Quine, T. A.; Wu, X. C.; Song, Z. L. Bedrock geochemistry influences vegetation growth by regulating the regolith water holding capacity. *Nature Communications* **2020**, *11* (1), 9; DOI 10.1038/s41467-020-16156-1.

- (27) Tong, X.; Brandt, M.; Yue, Y.; Horion, S.; Wang, K.; De Keersmaecker, W.; Tian, F.; Schurgers, G.; Xiao, X.; Luo, Y. Increased vegetation growth and carbon stock in China karst via ecological engineering. *Nature Sustainability* **2018**, *1* (1), 44–50.
- (28) Abatzoglou, J. T.; Dobrowski, S. Z.; Parks, S. A.; Hegewisch, K. C. TerraClimate, a high-resolution global dataset of monthly climate and climatic water balance from 1958–2015. *Sci. Data* **2018**, *5* (1), 170191; DOI 10.1038/sdata.2017.191.
- (29) Dynarski, K. A.; Morford, S. L.; Mitchell, S. A.; Houlton, B. Z. Bedrock nitrogen weathering stimulates biological nitrogen fixation. *Ecology* **2019**, *100* (8), e02741.
- (30) Wu, J.; Joergensen, R. G.; Pommerening, B.; Chaussod, R.; Brookes, P. C. Measurement of soil microbial biomass c by fumigation extraction - an automated procedure. *Soil Biol Biochem* **1990**, *22* (8), 1167–1169.
- (31) Qin, S.; Chen, L.; Fang, K.; Zhang, Q.; Wang, J.; Liu, F.; Yu, J.; Yang, Y. Temperature sensitivity of SOM decomposition governed by aggregate protection and microbial communities. *Science Advances* **2019**, *5* (7), eaau1218.
- (32) Qu, L.; Wang, C.; Bai, E. Evaluation of the $^{18}\text{O}\text{-H}_2\text{O}$ incubation method for measurement of soil microbial carbon use efficiency. *Soil Biology and Biochemistry* **2020**, *145*, 107802.
- (33) Spohn, M.; Klaus, K.; Wanek, W.; Richter, A. Microbial carbon use efficiency and biomass turnover times depending on soil depth – Implications for carbon cycling. *Soil Biology and Biochemistry* **2016**, *96*, 74–81.
- (34) Quast, C.; Pruesse, E.; Yilmaz, P.; Gerken, J.; Schweer, T.; Yarza, P.; Peplies, J.; Glöckner, F. O. The SILVA ribosomal RNA gene database project: improved data processing and web-based tools. *Nucleic Acids Research* **2012**, *41* (D1), D590–D596.

(35) Kõljalg, U.; Nilsson, R. H.; Abarenkov, K.; Tedersoo, L.; Taylor, A. F. S.; Bahram, M.; Bates, S. T.; Bruns, T. D.; Bengtsson-Palme, J.; Callaghan, T. M.; Douglas, B.; Drenkhan, T.; Eberhardt, U.; Dueñas, M.; Grebenc, T.; Griffith, G. W.; Hartmann, M.; Kirk, P. M.; Kohout, P.; Larsson, E.; Lindahl, B. D.; Lücking, R.; Martín, M. P.; Matheny, P. B.; Nguyen, N. H.; Niskanen, T.; Oja, J.; Peay, K. G.; Peintner, U.; Peterson, M.; Põldmaa, K.; Saag, L.; Saar, I.; Schüßler, A.; Scott, J. A.; Senés, C.; Smith, M. E.; Suija, A.; Taylor, D. L.; Telleria, M. T.; Weiss, M.; Larsson, K.-H. Towards a unified paradigm for sequence-based identification of fungi. *Molecular Ecology* **2013**, *22* (21), 5271–5277.

(36) Li, H.; Yang, S.; Semenov, M. V.; Yao, F.; Ye, J.; Bu, R.; Ma, R.; Lin, J.; Kurganova, I.; Wang, X.; Deng, Y.; Kravchenko, I.; Jiang, Y.; Kuzyakov, Y. Temperature sensitivity of SOM decomposition is linked with a K-selected microbial community. *Global Change Biol* **2021**, *27* (12), 2763–2779.

(37) Ling, N.; Wang, T.; Kuzyakov, Y. Rhizosphere bacteriome structure and functions. *Nature Communications* **2022**, *13*, 836.

(38) Ho, A.; Di Lonardo, D. P.; Bodelier, P. L. E. Revisiting life strategy concepts in environmental microbial ecology. *Fems Microbiol Ecol* **2017**, *93* (3).

(39) Yao, F.; Yang, S.; Wang, Z.; Wang, X.; Ye, J.; Wang, X.; DeBruyn, J. M.; Feng, X.; Jiang, Y.; Li, H. Microbial taxa distribution is associated with ecological trophic cascades along an elevation gradient. *Frontiers in Microbiology* **2017**, *8*, 2071.

(40) Stone, B. W. G.; Dijkstra, P.; Finley, B. K.; Fitzpatrick, R.; Foley, M. M.; Hayer, M.; Hofmockel, K. S.; Koch, B. J.; Li, J.; Liu, X. J. A.; Martinez, A.; Mau, R. L.; Marks, J.; Monsaint-Queeney, V.; Morrissey, E. M.; Propster, J.; Pett-Ridge, J.; Purcell, A. M.; Schwartz, E.; Hungate, B. A. Life

history strategies among soil bacteria—dichotomy for few, continuum for many. *The ISME Journal* **2023**, *17* (4), 611–619.

(41) Li, J. Q.; Pei, J. M.; Fang, C. M.; Li, B.; Nie, M. Thermal adaptation of microbial respiration persists throughout long-term soil carbon decomposition. *Ecology Letters* **2023**, *26* (10), 1803–1814.

(42) Cotrufo, M. F.; Ranalli, M. G.; Haddix, M. L.; Six, J.; Lugato, E. Soil carbon storage informed by particulate and mineral-associated organic matter. *Nature Geoscience* **2019**, *12* (12), 989–+,

(43) Chen, X.; Hu, Y.; Xia, Y.; Zheng, S.; Ma, C.; Rui, Y.; He, H.; Huang, D.; Zhang, Z.; Ge, T.; Wu, J.; Guggenberger, G.; Kuzyakov, Y.; Su, Y. Contrasting pathways of carbon sequestration in paddy and upland soils. *Global Change Biol* **2021**, *27* (11), 2478–2490.

(44) Liang, C.; Amelung, W.; Lehmann, J.; Kästner, M. Quantitative assessment of microbial necromass contribution to soil organic matter. *Global Change Biol* **2019**, *25* (11), 3578–3590.

(45) Chen, L.; Fang, K.; Wei, B.; Qin, S.; Feng, X.; Hu, T.; Ji, C.; Yang, Y. Soil carbon persistence governed by plant input and mineral protection at regional and global scales. *Ecology Letters* **2021**, *24* (5), 1018 – 1028.

(46) Wang, S.; Jia, Y.; Liu, T.; Wang, Y.; Liu, Z.; Feng, X. Delineating the role of calcium in the large-scale distribution of metal-bound organic carbon in soils. *Geophysical Research Letters* **2021**, *48* (10), e2021GL092391.

(47) Peng, S.; He, N.; Yu, G.; Wang, Q. Aboveground biomass estimation at different scales for subtropical forests in China. *Botanical Studies* **2017**, *58* (1), 45.

(48) Liu, S.; García-Palacios, P.; Tedersoo, L.; Guirado, E.; van der Heijden, M. G. A.; Wagg, C.; Chen, D.; Wang, Q.; Wang, J.; Singh, B. K.; Delgado-Baquerizo, M. Phylotype diversity within soil fungal functional groups drives ecosystem stability. *Nature Ecology & Evolution* **2022**, *6* (7), 900 –

909.

(49) Gupta, V. V. S. R.; Germida, J. J. Soil aggregation: Influence on microbial biomass and implications for biological processes. *Soil Biology and Biochemistry* **2015**, *80*, A3 – A9.

(50) Saifuddin, M.; Bhatnagar, J. M.; Segrè, D.; Finzi, A. C. Microbial carbon use efficiency predicted from genome-scale metabolic models. *Nature Communications* **2019**, *10* (1), 3568.

(51) Whitaker, J.; Ostle, N.; McNamara, N. P.; Nottingham, A. T.; Stott, A. W.; Bardgett, R. D.; Salinas, N.; Ccahuana, A. J. Q.; Meir, P. Microbial carbon mineralization in tropical lowland and montane forest soils of Peru. *Frontiers in Microbiology* **2014**, *5*, 720; DOI 10.3389/fmicb.2014.00720.

(52) Nottingham, A. T.; Meir, P.; Velasquez, E.; Turner, B. L. Soil carbon loss by experimental warming in a tropical forest. *Nature* **2020**, *584* (7820), 234 – 237.

(53) Cui, Y.; Hu, J.; Peng, S.; Delgado-Baquerizo, M.; Moorhead, D. L.; Sinsabaugh, R. L.; Xu, X.; Geyer, K. M.; Fang, L.; Smith, P.; Peñuelas, J.; Kuzyakov, Y.; Chen, J. Limiting Resources Define the Global Pattern of Soil Microbial Carbon Use Efficiency. *Advanced Science* **2024**, *11* (35), 2308176.

(54) Fernández-Ugalde, O.; Virto, I.; Barré, P.; Apesteguía, M.; Enrique, A.; Imaz, M. J.; Bescansa, P. Mechanisms of macroaggregate stabilisation by carbonates: Implications for organic matter protection in semi-arid calcareous soils. *Soil Res* **2014**, *52* (2), 180 – 192.

(55) Zamanian, K.; Pustovoytov, K.; Kuzyakov, Y. Pedogenic carbonates: Forms and formation processes. *Earth-Science Reviews* **2016**, *157*, 1 – 17.

(56) Chen, H.; Jing, Q.; Liu, X.; Zhou, X.; Fang, C.; Li, B.; Zhou, S.; Nie, M. Microbial respiratory thermal adaptation is regulated by r-/K-strategy dominance. *Ecology Letters* **2022**, *25* (11), 2489 –

2499.

(57) Loepmann, S.; Blagodatskaya, E.; Pausch, J.; Kuzyakov, Y. Substrate quality affects kinetics and catalytic efficiency of exo-enzymes in rhizosphere and detritosphere. *Soil Biology and Biochemistry* **2016**, *92*, 111 – 118.

(58) Lammirato, C.; Miltner, A.; Wick, L. Y.; Kästner, M. Hydrolysis of cellobiose by β -glucosidase in the presence of soil minerals – Interactions at solid–liquid interfaces and effects on enzyme activity levels. *Soil Biology and Biochemistry* **2010**, *42* (12), 2203–2210.

(59) Ye, C.; Huang, W.; Hall, S. J.; Hu, S. Association of Organic Carbon With Reactive Iron Oxides Driven by Soil pH at the Global Scale. *Global Biogeochemical Cycles* **2022**, *36* (1), e2021GB007128.

(60) Larjavaara, M.; Lu, X.; Chen, X.; Vastaranta, M. Impact of rising temperatures on the biomass of humid old-growth forests of the world. *Carbon Balance and Management* **2021**, *16* (1), 31.

(61) Dontsova, K.; Balogh-Brunstad, Z.; Chorover, J. Plants as Drivers of Rock Weathering. In *Biogeochemical Cycles*; Dontsova, K., Balogh-Brunstad, Z., Roux, G. L., Eds.; American Geophysical Union: New Jersey 2020; pp 33 – 58.

(62) Zhao, X.; Yang, Y.; Shen, H.; Geng, X.; Fang, J. Global soil-climate-biome diagram: linking surface soil properties to climate and biota. *Biogeosciences* **2019**, *16* (14), 2857 – 2871.

(63) Zimmerman, A. R.; Ahn, M.Y. Organo-Mineral–Enzyme Interaction and Soil Enzyme Activity. In *Soil Enzymology*; Shukla, G., Varma, A., Eds.; Springer: Berlin 2011; pp 271 – 292.

(64) Lavallee, J. M.; Soong, J. L.; Cotrufo, M. F. Conceptualizing soil organic matter into particulate and mineral-associated forms to address global change in the 21st century. *Global Change Biol* **2020**, *26* (1), 261 – 273.

- (65) Fan, X.; Gao, D.; Zhao, C.; Wang, C.; Qu, Y.; Zhang, J.; Bai, E. Improved model simulation of soil carbon cycling by representing the microbially derived organic carbon pool. *The ISME Journal* **2021**, *15* (8), 2248 – 2263.
- (66) Xiao, K.Q.; Liang, C.; Wang, Z.; Peng, J.; Zhao, Y.; Zhang, M.; Zhao, M.; Chen, S.; Zhu, Y.-G.; Peacock, C. L. Beyond microbial carbon use efficiency. *National Science Review* **2024**, *11* (4); DOI 10.1093/nsr/nwae059.
- (67) Dong, H.; Huang, L.; Zhao, L.; Zeng, Q.; Liu, X.; Sheng, Y.; Shi, L.; Wu, G.; Jiang, H.; Li, F.; Zhang, L.; Guo, D.; Li, G.; Hou, W.; Chen, H. A critical review of mineral–microbe interaction and co-evolution: mechanisms and applications. *National Science Review* **2022**, *9* (10); DOI 10.1093/nsr/nwac128.
- (68) He, P.; Zhang, Y.; Shen, Q.; Ling, N.; Nan, Z. Microbial carbon use efficiency in different ecosystems: A meta-analysis based on a biogeochemical equilibrium model. *Global Change Biol* **2023**, *29* (17), 4758 – 4774.
- (69) Beerling, D. J.; Kantzas, E. P.; Lomas, M. R.; Wade, P.; Eufrazio, R. M.; Renforth, P.; Sarkar, B.; Andrews, M. G.; James, R. H.; Pearce, C. R.; Mercure, J.F.; Pollitt, H.; Holden, P. B.; Edwards, N. R.; Khanna, M.; Koh, L.; Quegan, S.; Pidgeon, N. F.; Janssens, I. A.; Hansen, J.; Banwart, S. A. Potential for large-scale CO₂ removal via enhanced rock weathering with croplands. *Nature* **2020**, *583* (7815), 242 – 248.
- (70) Xu, T. T.; Yuan, Z. Q.; Vicca, S.; Goll, D. S.; Li, G. C.; Lin, L. X.; Chen, H.; Bi, B. Y.; Chen, Q.; Li, C. L.; Wang, X.; Wang, C.; Hao, Z. Q.; Fang, Y. T.; Beerling, D. J. Enhanced silicate weathering accelerates forest carbon sequestration by stimulating the soil mineral carbon pump. *Global Change Biol* **2024**, *30* (8), e17464.